Local structure of Pt and Pd ions in $Ce_{1-x}Ti_xO_2$: X-ray diffraction, x-ray photoelectron spectroscopy, and extended x-ray absorption fine structure

Tinku Baidya,[1] K. R. Priolkar,[2] P. R. Sarode,[2] M. S. Hegde,[1,a)] K. Asakura,[3] G. Tateno,[4] and Y. Koike[4]
[1]*Solid State and Structural Chemistry Unit, Indian Institute of Science, Bangalore 560012, India*
[2]*Department of Physics, Goa University, Taleigao Plateau, Goa 403206, India*
[3]*Catalysis Research Centre, Hokkaido University, Sapporo 001-0021, Japan*
[4]*Photon Factory, Tsukuba-shi, Ibaraki-ken 305-0801, Japan*

(Received 29 November 2007; accepted 11 January 2008; published online 28 March 2008)

$Ce_{1-x-y}Ti_xPt_yO_{2-\delta}$ ($x=0.15$; $y=0.01$) and $Ce_{1-x-y}Ti_xPd_yO_{2-\delta}$ ($x=0.25$; $y=0.02$ and 0.05) are found to be good CO oxidation catalysts [T. Baidya *et al.*, J. Phys. Chem. B **110**, 5262 (2006); T. Baidya *et al.*, J. Phys. Chem. C **111**, 830 (2007)]. A detailed structural study of these compounds has been carried out by extended x-ray absorption fine structure along with x-ray diffraction and x-ray photoelectron spectroscopy. The gross cubic fluorite structure of CeO_2 is retained in the mixed oxides. Oxide ion sublattice around Ti as well as Pt and Pd ions is destabilized in the solid solution. Instead of ideal eight coordinations, Ti, Pd, and Pt ions have 4+3, 4+3, and 3+4 coordinations creating long and short bonds. The long Ti–O, Pd–O, and Pt–O bonds are ~2.47 Å (2.63 Å for Pt–O) which are much higher than average Ce–O bonds of 2.34 Å. © *2008 American Institute of Physics*. [DOI: 10.1063/1.2841365]

INTRODUCTION

Ionically dispersed Pd, Cu, Pt, and Rh in CeO_2 have shown higher catalytic activity compared to the impregnated catalysts.[1–6] Interaction of noble metal ions with CeO_2 support has played a crucial role in redox reactions bringing down the catalytic reaction temperature and decrease in activation energy. Oxygen storage capacity (OSC), a well known property of CeO_2, acts as a buffer medium of oxygen required in redox reaction. Noble metal ion substitution in CeO_2 promotes reduction of the support at much lower temperature. However, the amount of lattice oxygen taking part in the redox reaction is small in pure CeO_2.

Modification of CeO_2 by the substitution of smaller cation like Zr or Ti has shown enhancement of OSC. Zr substitution in CeO_2 forming $Ce_{1-x}Zr_xO_2$ solid solution has been extensively studied in the literature.[7–11] Ti ion substitution in CeO_2 forming $Ce_{1-x}Ti_xO_2$ solid solution has been reported by us recently.[12] In this oxide both Ce and Ti have four long+four short bond with oxygen compared to ideal eight coordinations in CeO_2.[13] Since both Ti and Ce ions are reducible, higher catalytic activity was observed in the presence of Pt and Pd ion.[12,14] Therefore, understanding of the local structure of Pt and Pd ions in this mixed oxide is important. However, at 1–2 at. % Pt or Pd ion substitution in $Ce_{1-x}Ti_xO_2$, it is often difficult to ascertain the structure by x-ray diffraction (XRD) alone.

Here we report local structure of Pt and Pd ions substituted in $Ce_{1-x}Ti_xO_2$ by a detailed XRD, x-ray photoelectron spectroscopy (XPS), and extended x-ray absorption fine structure EXAFS study.

a)Author to whom correspondence should be addressed. Electronic mail: mshegde@sscu.iisc.ernet.in. Tel.: +91-80-2293-2614. FAX: +91-80-2360-1310.

EXPERIMENTAL SECTION

1 at. % $Pt/Ce_{0.85}Ti_{0.15}O_2$ was prepared by the solution combustion method taking $(NH_4)_2Ce(NO_3)_6 \cdot 6H_2O$, $Pt(NH_3)_3(NO_3)_2$ (ABCR, France), $TiO(NO_3)_2$, and glycine in the mole ratio 0.8415:0.01:0.1485:2:2.42. In a typical preparation, 3 g $(NH_4)_2Ce(NO_3)_6 \cdot 6H_2O$, 0.0252 g $Pt(NH_3)_4(NO_3)_2$, 0.1823 g $TiO(NO_3)_2$ (in solution), and 1.1814 g glycine were taken in a 300 ml Pyrex dish. $TiO(NO_3)_2$ is prepared from $TiCl_4$ and the detailed procedure has been published somewhere else.[12]

$Ce_{0.73}Ti_{0.25}Pd_{0.02}O_{2-\delta}$ was prepared by solution combustion method taking $(NH_4)_2Ce(NO_3)_6$, $PdCl_2$, $TiO(NO_3)_2$ (in solution), and glycine in the molar ratio 0.73:0.02:0.0.25:2.42. For usual preparation, 5 g $(NH_4)_2Ce(NO_3)_6$, 0.586 g $TiO(NO_3)_2$, 0.044 g $PdCl_2$, and 2.08 g $C_2H_5NO_2$ were taken. The solution is heated in the furnace at 350 °C which gives product as described in the earlier study.[14]

XRD data of all the mixed oxides and the Pt-substituted oxides were recorded in a Philips X'Pert diffractometer at a scan rate of 0.5 deg min^{-1} with 0.02 deg step size in the 2θ range between 20 and 100 deg. The refinement was done using FULLPROF-FP2K program[15] varying 17 parameters, such as overall scale factor and background parameters, along with oxygen occupancy.

XPS spectra of the prepared compounds were recorded in an ESCA-3 Mark II spectrometer (VG Scientific Ltd., England) using Al K_α radiation (1486.6 eV). Binding energies were calibrated with respect to C(1*s*) at 285 eV with a precision of ±0.1 eV. For XPS analysis the power samples were made into 0.5 mm thick, 8 mm diameter pellets and placed into an ultrahigh vacuum chamber at 10^{-9} Torr hous-

ing the analyzer. The obtained spectra were curve fitted with Gaussian peaks after subtracting a linear background.

Ti K, Pt L_{III}, and Pd K edge EXAFS spectra in catalyst and reference samples were recorded at room temperature in the transmission mode with Si(311) and Si(111) double-crystal monochromators at NW10A and BL9A beamlines, respectively, at Photon Factory, Japan.[16,17] EXAFS was scanned from 4.7 to 5.6 keV, from 11 to 12 keV for Pt EXAFS, and from 24.2 to 25.6 keV for Pd EXAFS spectra. The photon energy was calibrated for each scan with the first inflection point of the absorption edge in respective metal foil. Both the incident (I_0) and transmitted (I) synchrotron beam intensities were measured simultaneously using ionization chamber filled with appropriate gases. The absorbers were made by pressing the fine powder samples into pellets of 10 mm diameter with boron nitride. To avoid the sample thickness effect, the total μx was restricted to a value $\leqslant 3$ by adjusting the thickness of the absorber pellet where μ is the absorption coefficient and x is the sample thickness.[18]

EXAFS data analysis was done using IFEFFIT program. The value of amplitude reduction factor (S_0^2) is deduced from the EXAFS spectra of respective metals with known crystal structural data.[19] The theoretical calculation of back-scattering amplitude and phase shift functions is obtained by using FEFT (6.01) program.[20] The experimental EXAFS data were fitted with the theoretical EXAFS function using FEFFIT program.[21]

RESULTS AND DISCUSSION

XRD study

XRD was carried out to see whether platinum ions are substituted into the $Ce_{0.85}Ti_{0.15}O_2$ matrix in $Pt/Ce_{0.85}Ti_{0.15}O_2$ catalyst. Figure 1(a) shows the XRD pattern of as-prepared 1 at. % $Pt/Ce_{0.85}Ti_{0.15}O_2$ and 1 at. % Pt impregnated over $Ce_{0.85}Ti_{0.15}O_2$ with ten times enlarged in the Y scale. The pattern can be indexed to the fluorite structure. Observed, calculated, and difference XRD patterns of 1 at. % $Pt/Ce_{0.85}Ti_{0.15}O_2$ are shown in Fig. 1(b). The R_{Bragg}, R factor, and χ^2 values are 1.75, 1.81, and 1.04, respectively. Keeping all the parameters the same and Pt ion occupancy equal to 0.0, R_{Bragg}, R_F, and χ^2 were 2.25, 1.64, and 1.15, respectively. The increase in R factors is significant. This test confirms Pt ion substitution for Ti/Ce sites in the lattice. Therefore, the present model which considers Pt ion substitution at Ce^{4+} site in $Ce_{1-x}Ti_xO_2$ lattice is possible. The lattice parameter of $Ce_{0.85}Ti_{0.15}O_2$ is 5.4032(2) Å and in the 1 at. % Pt ion substituted $Ce_{0.85}Ti_{0.15}O_2$, lattice parameter changes to 5.4052(3) Å. There are no impurity peaks due to the presence of platinum metal or oxides. This is further confirmed by recording 1 at. % Pt impregnated over $Ce_{0.85}Ti_{0.15}O_2$ where intense Pt(111) peak is observed. In the impregnated compound Pt(111) peak is clearly observed, as indicated in Fig. 1(a).

1% Pt-substituted catalyst was reduced in 5 % H_2/Ar gas at 300 °C for 1 h. Color changed from gray to black. Figure 2 shows the XRD pattern of the reduced sample with magnification in the Y scale. Pt(111) peak at 2θ=39.8 is not observed. This shows that short duration reduction does not allow Pt metal atoms sintering to metal particles. We believe that atoms are retained in the same sites as in the unreduced samples. A similar experiment has been reported in the literature as an evidence for Pd ion substitution in perovskite lattice.[22–24] However, reduction of Pt ion in H_2 and easy reoxidation in O_2 have been shown by XPS study earlier.[12]

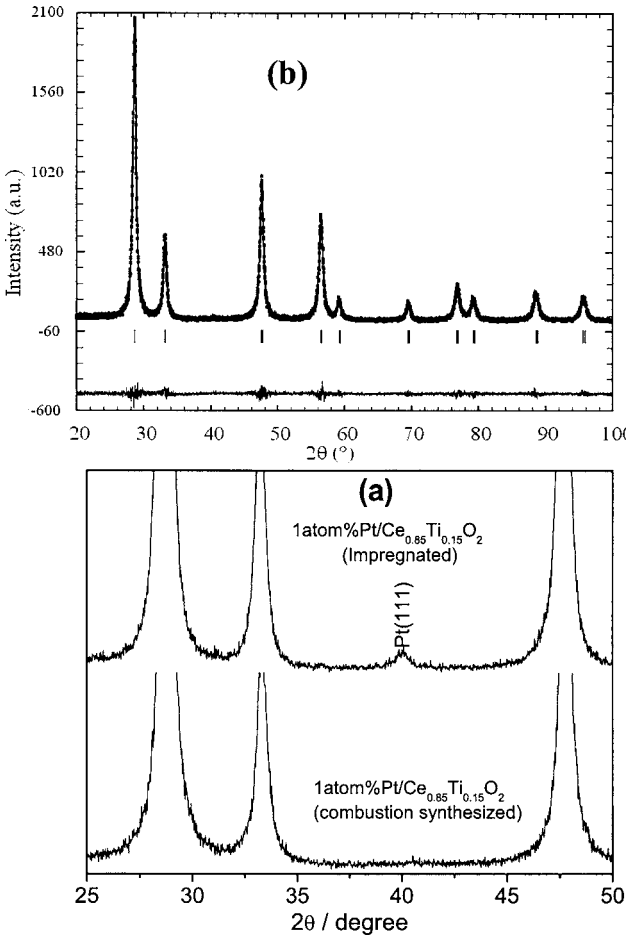

FIG. 1. (a) Ten times enlarged XRD pattern of 1 at. % $Pt/Ce_{0.85}Ti_{0.15}O_2$ and 1 at. % $Pt/Ce_{0.85}Ti_{0.15}O_2$ (impregnated) and (b) Rietveld refined 1 at. % $Pt/Ce_{0.85}Ti_{0.15}O_2$.

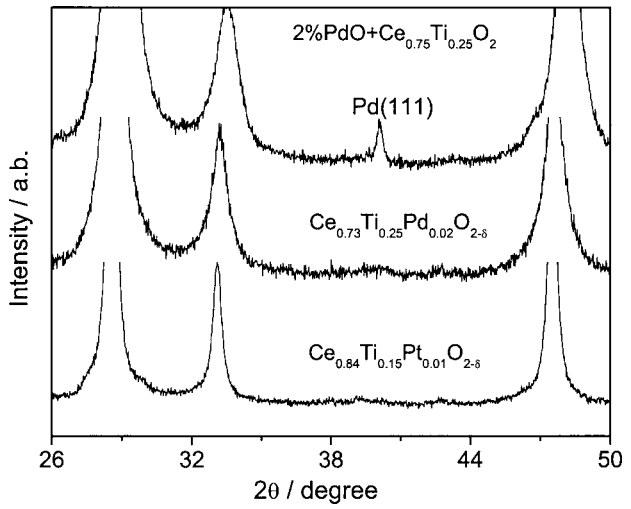

FIG. 2. XRD pattern of 1 at. % $Pt/Ce_{0.85}Ti_{0.15}O_2$ (at 300 °C), 2 at. % $Pd/Ce_{0.75}Ti_{0.25}O_2$ (at 500 °C), and 2% PdO+$Ce_{0.75}Ti_{0.25}O_2$ (at 500 °C) reduced in 5% H_2+95% Ar gas.

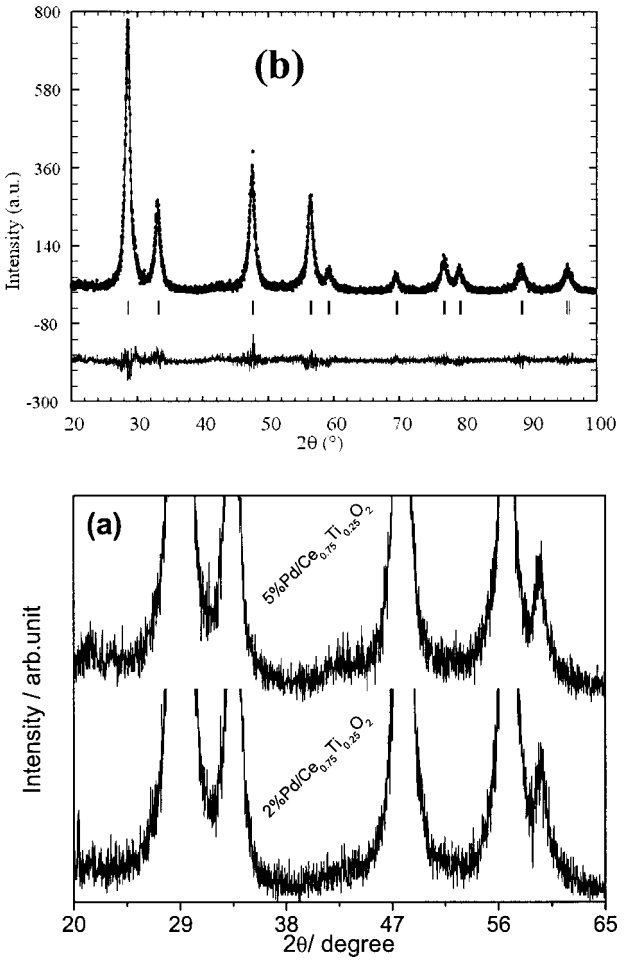

FIG. 3. (a) Ten times enlarged XRD pattern of 2 and (b) 5 at. % $Pd/Ce_{0.75}Ti_{0.25}O_2$.

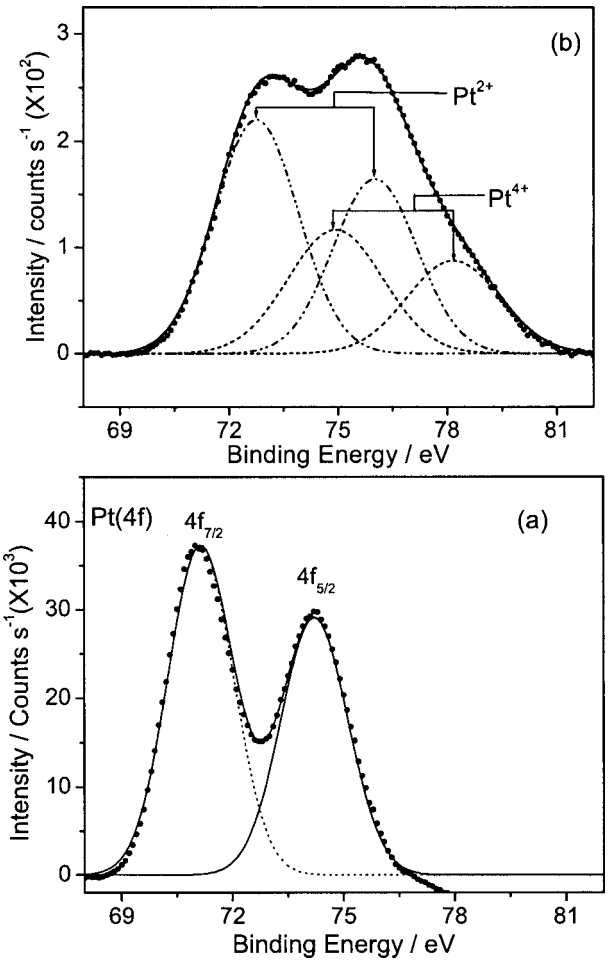

FIG. 4. Pt(4*f*) core level spectra in (a) Pt metal foil and (b) 1 at. % $Pt/Ce_{0.85}Ti_{0.15}O_2$.

Figure 3(a) shows the XRD pattern of as-prepared 2 and 5 at. % $Pd/Ce_{0.75}Ti_{0.25}O_2$ which is ten times enlarged in the *Y* scale. The patterns show fluorite phase of the catalysts. No intensity peak due to Pd metal particle or PdO can be observed. Figure 3(b) shows the Rietveld refined XRD profile of 5 at. % $Pd/Ce_{0.75}Ti_{0.25}O_2$. R_{Bragg}, *R* factor, and χ^2 values are 1.94, 2.90, and 1.44 for 2 at. % $Pd/Ce_{0.75}Ti_{0.25}O_2$ and 3.57, 2.36, and 1.29 for 5 at. % $Pd/Ce_{0.75}Ti_{0.25}O_2$, respectively. Lattice parameter values are, respectively, 5.3992(6) and 5.4082(5) Å. The increase in lattice parameter is 5% Pd substituted compound due to higher ionic radii of Pd^{2+} ion compared to smaller Ti^{4+} ion which gets substituted by Pd^{2+} ion.

Similar to Pt- substituted catalyst, in Fig. 2 the XRD pattern of $Ce_{0.73}Ti_{0.25}Pd_{0.02}O_{2-\delta}$ and 2 at. % PdO $+Ce_{0.75}Ti_{0.25}O_2$ (mixture) reduced in H_2 is shown. Pd(111) metal peak at $2\theta=40.2$ is not observed in the substituted catalyst whereas the same gives a prominent peak in 2 at. % $PdO+Ce_{0.75}Ti_{0.25}O_2$.

XPS study

The valence state of platinum species in the $Ce_{1-x}Ti_xO_2$ support was determined by XPS of Pt(4*f*) core level spectra. Pt(4*f*) core level region in pt metal foil and as-prepared 1 at. % $Pt/Ce_{0.85}Ti_{0.15}O_2$ is given in Fig. 4. Pt^0 in Pt metal particles shows $4f_{7/2,5/2}$ at 71.1 and 74.3 eV, respectively [Fig. 4(a)]. However, Pt spectra are very broad in the oxide support. Therefore, Pt(4*f*) spectrum was deconvoluted into sets of spin-orbit doublets for different oxidation states of Pt. In 1% $Pt/Ce_{0.85}Ti_{0.15}O_2$, the Pt(4*f*) region [Fig. 4(b)] was deconvoluted into two sets of spin-orbit doublets because significant intensity due to metallic platinum was not observed even after ten times magnification in XRD. Accordingly, the peaks at 72.8, 76 and 75, 78.2 eV are attributed to

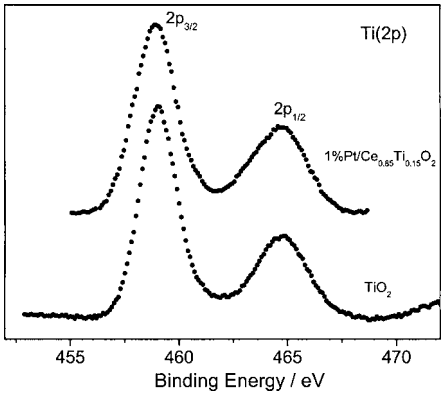

FIG. 5. Ti(2*p*) core level spectra in (a) TiO_2 and (b) 1 at. % $Pt/Ce_{0.85}Ti_{0.15}O_2$.

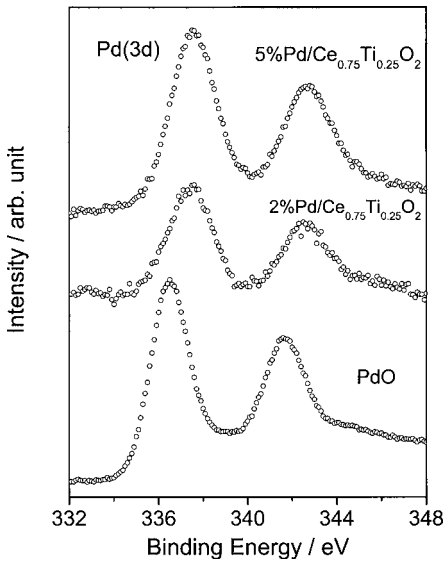

FIG. 6. Pd(3*d*) core level spectra in PdO, 2 at. % $Pd/Ce_{0.75}Ti_{0.25}O_2$, and 5 at. % $Pd/Ce_{0.75}Ti_{0.25}O_2$.

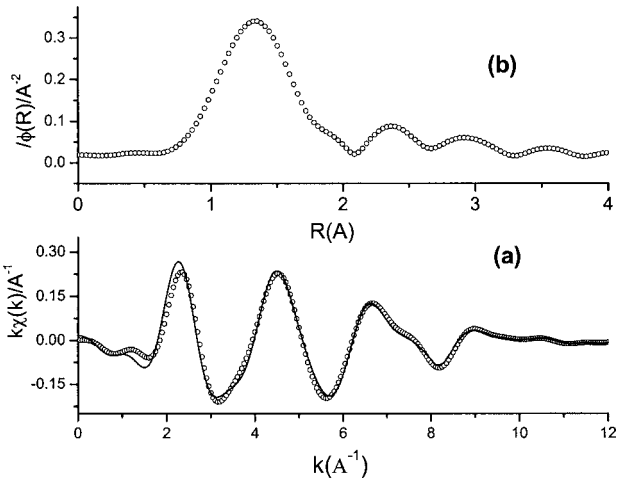

FIG. 7. (a) Fourier transformed EXAFS spectra at the Ti *K* edge in 1 at. % $Pt/Ce_{0.85}Ti_{0.15}O_2$ and (b) magnitude of k^2 weighted EXAFS spectra in 1 and 2 at. % $Pt/Ce_{0.85}Ti_{0.15}O_2$.

Pt in +2 and +4 oxidation states, respectively. About ~65% Pt are in +2 state and the rest is in +4 state in 1 at. % $Pt/Pt_{0.85}Ti_{0.15}O_{2-\delta}$.

The Ti(2*p*) spectrum of pure TiO_2 and as-prepared 1 at. % $Pt/Ce_{0.85}Ti_{0.15}O_2$ is shown in Fig. 5. Binding energies of Ti($2p_{3/2,1/2}$) at 459.0 and 464.8 eV in TiO_2 correspond to Ti in 4+ state [Fig. 5(a)]. The Ti($2p_{3/2,1/2}$) peaks in as-prepared 1 at. % $Pt/Ce_{0.85}Ti_{0.15}O_2$ are observed at 458.8 and 464.7 eV [Fig. 5(b)] and therefore, Ti is essentially in 4+ state in the Pt-substituted catalysts. Similarly, Ce is also present in the 4+ state in all the compounds.

Figure 6 shows the Pd(3*d*) core level spectra in PdO, as-prepared 2 and 5 at. % $Pd/Ce_{0.75}Ti_{0.25}O_2$. The binding energy of Pd($3d_{5/2}$) in PdO is 336.4 eV corresponding to 2 + state. Pd($3d_{5/2}$) is observed at 337.7 eV in as-prepared 2 and 5 at. % $Pd/Ce_{0.75}Ti_{0.25}O_2$. $PdCl_2$ is observed at 338.0 eV.[25] Therefore, Pd ion is in +2 state, but it is more ionic in $Ce_{0.75}Ti_{0.25}O_2$ than in PdO. Similarly, both Ti and Ce ions showing similar spectra are found to be in 4+ state.

EXAFS study

The k^2 weighted Fourier transform (FT) of Ti *K*-edge EXAFS in 1% $Pt/Ce_{0.85}Ti_{0.15}O_2$ is presented in Fig. 7(a). These spectra are very similar to those of Ti EXAFS in $Ce_{1-x}Ti_xO_2$ solid solutions[13] where we had reported that the oxygen coordination around Ti is distorted in these solid solutions. From experimental data analysis as well as first prin-

TABLE I. EXAFS analysis in $Pt/CeTiO_2$ at Ti *K* edge and Pt L_{III} edge.

Sample	Coordination shell	CN	*R*	σ^2
		Ti *K* edge		
1% $Pt/Ce_{0.85}Ti_{0.15}O_2$	Ti–O	4	1.897 ± 0.06	0.005 ± 0.001
		4	2.50 ± 0.02	0.023 ± 0.006
	Ti–Ti	1.8	2.98 ± 0.03	0.010 ± 0.004
	Ti–Ce	10.2	3.52 ± 0.06	0.03 ± 0.01
		Pt L_{III} edge		
1% $Pt/Ce_{0.85}Ti_{0.15}O_2$	Pt–O	2.9 ± 0.1	0.004 ± 0.003	0.0049 ± 0.0004
		3.9 ± 0.1	2.63 ± 0.04	0.041 ± 0.009
	Pt–Pt	3.6 ± 0.6	2.768 ± 0.002	0.0049 ± 0.0002
	Pt–Ti	1.1 ± 0.3	3.12 ± 0.02	0.016 ± 0.003
	Pt–Ce	5.1 ± 0.7	3.54 ± 0.01	0.020 ± 0.002
PT	Pt–Pt	12.0	2.762 ± 0.004	0.009 ± 0.001
		6.0	3.901 ± 0.005	0.013 ± 0.003
		48.0	4.138 ± 0.005	0.016 ± 0.003
		24.0	4.778 ± 0.006	0.015 ± 0.002
PtO_2	Pt–O	5.6 ± 0.2	1.989 ± 0.004	0.002 ± 0.001
	Pt–Pt	3.7 ± 0.2	3.153 ± 0.002	0.006 ± 0.001
	Pt–Pt	7.6 ± 0.4	3.556 ± 0.006	0.014 ± 0.008
	Pt–O	4.5 ± 0.6	3.695 ± 0.006	0.005 ± 0.002

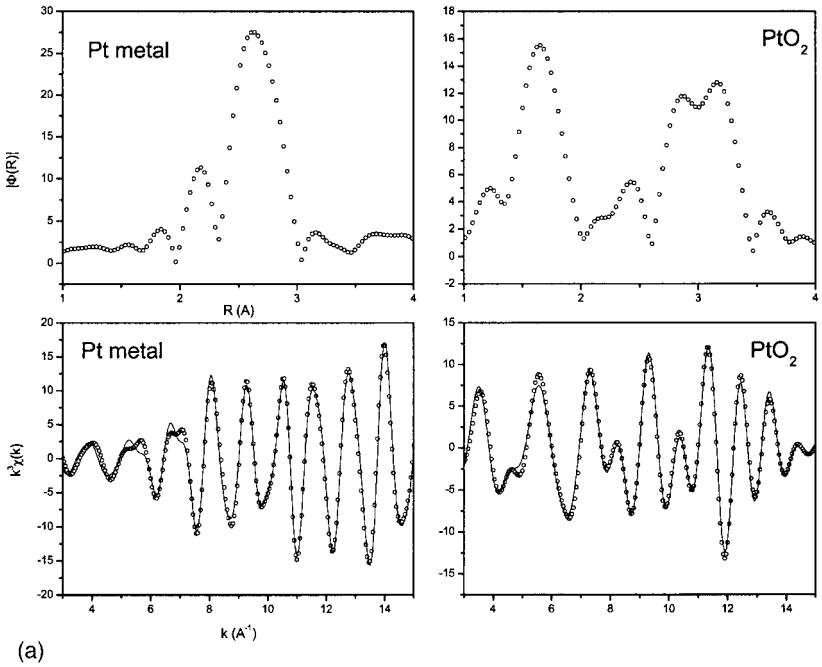

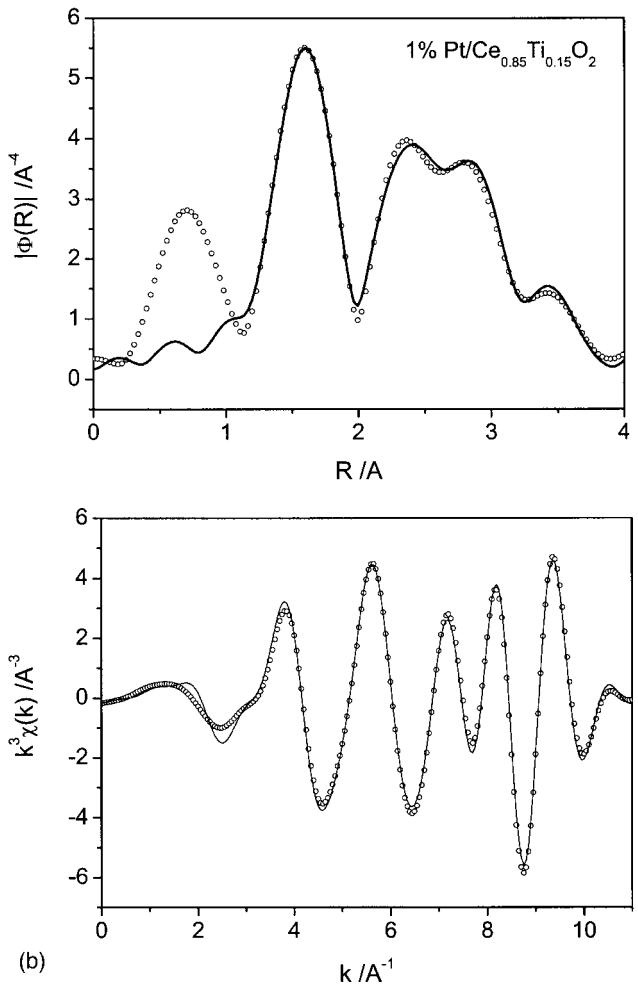

FIG. 8. (a) Magnitude of FT and corresponding backtransforms of Pt L_{III} edge in Pt metal foil and PtO_2 and (b) backtransformed k^3 weighted EXAFS with fit and magnitude of FT of Pt L_{III} edge in 1 at. % $Pt/Ce_{0.85}Ti_{0.15}O_2$.

cipal theoretical calculations it was found that of the eight O's surrounding the metal ion in fluorite structure, four come closer and four move away. The weighted EXAFS data in the k range 2–10 $Å^{-1}$ were transformed to R space and was fitted to the same 4+4 coordination model using Ti–O correlations and Ti–Ti and Ti–Ce coordination shells. The resultant backtransformed data along with the fit are presented in Fig. 7(b). The values of bond lengths and Debye–Waller terms are presented in Table I. When coordination was taken as 8, 6+2 or 4+2+2 fitting was poor.

Figure 8(a) shows the k^3 weighted FT of the Pt L_{III} EXAFS spectra of Pt metal and PtO_2 along with their inverse

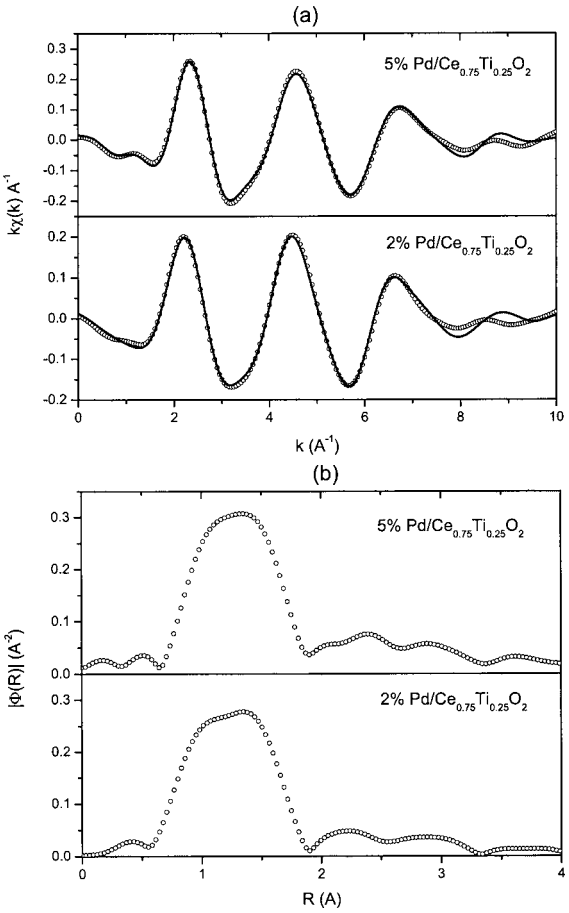

FIG. 9. (a) Fourier transformed EXAFS spectra at the Ti *K* edge in 2 and 5 at. % $Pd/Ce_{0.75}Ti_{0.25}O_2$ and (b) magnitude of k^2 weighted EXAFS spectra in 1 and 2 at. % $Pt/Ce_{0.85}Ti_{0.15}O_2$.

transforms. The Fourier transforms are not corrected for phase shift and hence the peaks are shifted to lower *R* values. However, as mentioned above, the values of bond distance quoted in the text and table are corrected for phase shift. For Pt metal foil, the Pt–Pt scattering peak is seen at 2.76 Å. In addition to it, a small peak on the lower *R* side of the main peak can be seen. This is caused by both the *k*-dependent behavior of backscattering amplitude and nonlinearly in the phase shift function. Pt–O correlation in PtO_2 appears at about 1.99 Å and a Pt–Pt correlation is observed at an average distance of 3.15 Å. The values of bond distance, coordination number, and Debye–Waller factors obtained from fitting the EXAFS data in the *R* range 1–4 Å are presented in Table I. These values agree well with the structural data of Pt and PtO_2.

In the case of 1% $Pt/Ce_{0.85}Ti_{0.15}O_2$ [Fig. 8(b)], a strong peak at about 1.5 Å (phase shift uncorrected) is observed which is absent in Pt metal. This correlation is attributed to the Pt–O bond at 2.0 Å. Further a broad structure with at least three distinct maxima is seen in the range 2–4 Å. This broad structure distinctly consists of at least three correlations and it is similar to that observed in 1% Pt/CeO_2.[26] But there are important differences in the two spectra particularly in weighting of the doublet structure, positions of the maxima as well as in the strength of the first Pt–O correlation at 2 Å. therefore, in $Pt/CeTiO_2$ catalyst although Pt could be in similar environment as that in Pt/CeO_2 the nature of correlations could be different. This could be due to distorted ceria-titania matrix that Pt finds itself in $Pt/CeTiO_2$. Therefore, to fit the EXAFS data, a model wherein Pt ion is substituted for Ce/Ti ion in $Pt/Ce_{0.8}Ti_{0.2}O_2$ structure forming a solid solution of the type $Pt_{0.01}Ce_{0.79}Ti_{0.2}O_{2-\delta}$ was considered. This model gave a good fit and the fitted parameters obtained are listed in Table I. In the solid solution phase, Pt has ~3+4 oxygen coordination at 2.0 and 2.63 Å in the catalyst. If Pt ions are substituted for Ce^{4+} sites, the first coordination around Pt ion will be of oxide ions. In the case of $Ce_{1-x}Ti_xO_2$, Ce has distorted oxygen coordination around it with four oxygen ions coming closer and four moving away. Accordingly, the coordination of ~7 (4 short+3 long) for the Pt–O bond in the catalyst can be understood to be due to substitution of Pt^{2+} ions for Ce^{4+} ions just as Ti^{4+} ion in CeO_2 accounting for overall oxide ion vacancy. Since 65% of Pt ions is in lower oxidation state, oxide ion vacancy is expected and the observed lower coordination supports this. Further, Pt–Pt, Pt–Ti, and Pt–Ce correlation were obtained at 2.76, 3.12, and 3.53 Å, respectively. These correlations indicate the presence of Pt ion in fluorite lattice. The total coordination number obtained was about 10 which is close to that expected for Pt substitution for Ce ion in $(CeTi)O_2$ solid solution having fluorite structure. The Pt–Ce bond distance of 3.53 Å is also close to Ti–Ce distance (3.5 Å) obtained in $(CeTi)O_2$ solid solutions. However, the Pt–Pt coordination number (~4) is quite large. It must be mentioned here that while fitting, the coordination numbers were essentially kept fixed to their respective concentration ratio. In the case of Pt–Pt, Pt–Ti, and Pt–Ce, a good fit was obtained only for a combination of 4, 1, and 5, respectively.

The k^2 weighted FT of Ti *K*-edge EXAFS in 2 and 5 at. % $Pd/Ce_{0.75}Ti_{0.25}O_2$ is presented in Fig. 9(a). This spectrum is similar to those of Ti EXAFS in $Ce_{1-x}Ti_xO_2$ solid solutions.[13] The weighted EXAFS data in the *k* range 2–10 $Å^{-1}$ were transformed to *R* space and were fitted to the same 4+4 model using Ti–O correlations and Ti–Ti and Ti–Ce coordination shells. The resultant backtransformed data along with the fit are presented in Fig. 9(b). The values of bond lengths and Debye–Waller terms are presented in Table II. The second shell in the Ti–O coordination sphere is ~3. This is due to creation of oxide ion vacancy for lower valent Pd^{2+} ion substitution.

Figures 10(a) and 10(b) show background subtracted k^3-weighted Pd *K* EXAFS function with fit and its magnitude in Pd metal and PdO. The EXAFS spectrum of the catalyst is similar to that of PdO, indicating Pd to be in +2 state. The phase corrected values of EXAFS data are given in Table II. The FT of PdO shows three distinct peaks in the range 1–3.5 Å. It is known from the crystal structure data that in PdO, Pd ion is surrounded by four O ions at 2.02 Å and Pd ions at 2.67 and 3.08 Å with coordination numbers 2 and 4, respectively. These shells contribute to the first two peaks while the third peak has contributions from 8 neighbored Pd–O shell at 3.58 Å and 16 neighbored Pd–Pd shell at 3.72 Å. From the EXAFS data, we have shown local structure of Ce^{4+}, Ti^{4+}, and Pd^{2+} ions in Fig. 11. Ce^{4+} is found to have four Ce–O bonds of 2.30 Å and four Ce–O of 2.42 Å.[13]

TABLE II. EXAFS analysis in Pd metal, PdO, and $Pd/CeTiO_2$ at Ti *K* and Pd *K* edges.

Sample	Coordination shell	CN	*R*	σ^2
		Ti *K* edge		
2% $Pd/Ce_{0.75}Ti_{0.25}O_2$	Ti–O	4	1.925 ± 0.004	0.007 ± 0.001
		2.9 ± 0.5	2.48 ± 0.02	0.032 ± 0.006
	Ti–Ti	2.2 ± 0.6	3.05 ± 0.03	0.019 ± 0.005
	Ti–Ce	9.0 ± 0.2	3.67 ± 0.03	0.038 ± 0.006
5% $Pd/Ce_{0.75}Ti_{0.25}O_2$	Ti–O	4	1.903 ± 0.004	0.0064 ± 0.0007
		3.0 ± 0.4	2.42 ± 0.01	0.022 ± 0.004
	Ti–Ti	2.0 ± 0.7	3.15 ± 0.05	0.025 ± 0.009
	Ti–Ce	5.3 ± 0.2	3.82 ± 0.08	0.062 ± 0.01
	Ti–Pd	1.2 ± 0.4	3.20 ± 0.03	0.010 ± 0.001
		Pd *K* edge		
2% $Pd/Ce_{0.75}Ti_{0.25}O_2$	Pd–O	4.0 ± 0.02	2.007 ± 0.004	0.0028 ± 0.0004
		3.2 ± 0.6	2.47 ± 0.02	0.013 ± 0.003
	Pd–Pd	1.8 ± 0.1	3.059 ± 0.005	0.0048 ± 0.0005
	Pd–Ti	2.8 ± 0.4	2.89 ± 0.01	0.014 ± 0.002
	Pd–Ce	6.3 ± 0.4	3.330 ± 0.004	0.0097 ± 0.0004
Pd	Pd–Pd	12.0	2.747 ± 0.003	0.006 ± 0.001
		6.0	3.885 ± 0.002	0.009 ± 0.001
		48.0	4.120 ± 0.002	0.008 ± 0.001
		24.0	4.689 ± 0.004	0.050 ± 0.004
PdO	Pd–O	4.0	2.023 ± 0.005	0.002 ± 0.001
	Pd–Pd	2.0	2.694 ± 0.008	0.011 ± 0.003
	Pd–Pd	4.0	3.079 ± 0.009	0.005 ± 0.001
	Pd–O	8.0	3.581 ± 0.002	0.002 ± 0.001
	Pd–O/Pd	16.0	3.721 ± 0.009	0.006 ± 0.001

Both Ti^{4+} and Pd^{2+} ions have 4+3 coordination. Ti–O bond distances were 1.90 and 2.48 and Pd–O bonds were 2.0 and 2.47 Å. Oxide ion vacancy is obtained in the longer coordination sphere.

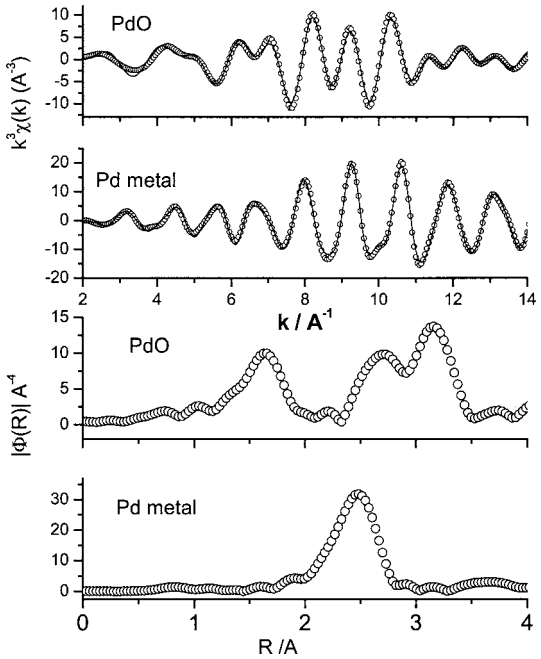

FIG. 10. Backtransform EXAFS with fit and magnitude of FT of Pd *K* edge in Pd and PdO.

In the case of catalyst sample, a strong peak at about 1.5 Å (phase shift uncorrected) is seen and can be attributed to Pd–O correlation with a bond length of 2.02 Å. The coordination number obtained from fitting this peak is about 4. The fit, however, is not very good especially in the higher *R* region where a small correlation, especially in the sample containing 5% Pd, can be seen. Further there is a broad structure extending from little over 2 to about 3.5 Å. This structure is different from the twin peak structure seen in PdO both in terms of peak position and relative heights, indicating the local structure around the metal ion to be different in catalyst from that in PdO. Therefore, the EXAFS was fitted to a model wherein Pd substitutes Ce ion in distorted fluorite

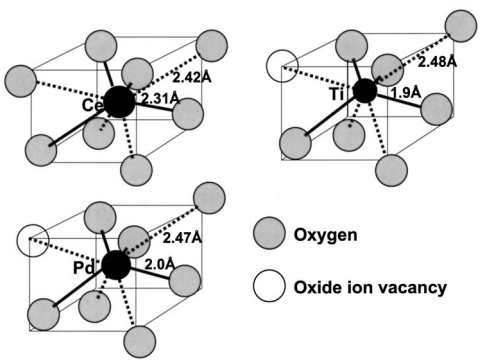

FIG. 11. Ball and stick model obtained from EXAFS fitting for the first coordination shell around Ce, Ti, and Pd ions in $Ce_{0.73}Ti_{0.25}Pd_{0.02}O_{2-\delta}$.

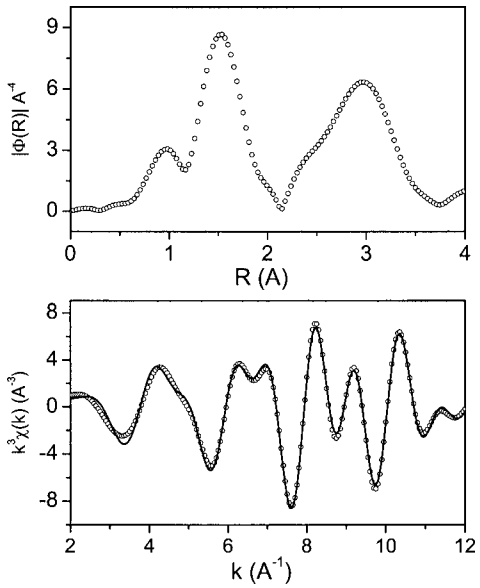

FIG. 12. Backtransform EXAFS with fit and magnitude of FT of Pd *K* edge in $Ce_{0.73}Ti_{0.25}Pd_{0.02}O_{2-\delta}$.

structure.[2] The fitting parameters obtained are presented in Table II and the fitted curves in the backtransformed *k* space along with those of Pd metal and PdO are presented in Fig. 12. It can be seen that the first peak in the magnitude of FT of EXAFS spectra can be fitted with two Pd–O correlations at 2.02 and 2.47 Å, respectively. The total coordination number is about 7 which can be expected due to substitution of lower valent Pd^{2+} ion in place of Ce^{4+} ion. Further, the twin peak structure can be fitted with three correlations, Pd–Ti, Pd–Pd, and Pd–Ce at 2.89, 3.06, and 3.3 Å, respectively. The obtained coordination numbers are also in accordance with atomic concentration of each of these ions as well as the total coordination number is close to 12, which is expected for second coordination in fluorite structure. This clearly confirms that in 2% Pd/$CeTiO_2$ Pd^{2+} ion substitutes Ce^{4+} in a distorted fluorite structure.

CONCLUSIONS

Pt is present in the +2 and +4 ionic state in $Ce_{1-x}Ti_xO_2$, whereas Pd in +2 state.

Coordination number as well as Pt–O and Pt–Pt or Pt–Ce/Ti distances in $Pt/Ce_{0.85}Ti_{0.15}O_2$ are different from those distances in Pt metal or PtO_2. Similarly, Pd substitution gives different bond distances in $Ce_{0.75}Ti_{0.25}O_2$.

1 at. % $Pt/Ce_{0.85}Ti_{0.15}O_2$ can be written as $Ce_{0.84}Ti_{0.15}Pt_{0.01}O_{2-\delta}$ with cubic fluorite structure. Similarly, 2 and 5 at. % $Pt/Ce_{0.75}Ti_{0.25}O_2$ can be written as $Ce_{0.73}Ti_{0.25}Pd_{0.02}O_{2-\delta}$ and $Ce_{0.7}Ti_{0.25}Pt_{0.05}O_{2-\delta}$, respectively.

ACKNOWLEDGMENTS

The authors from IISc and Goa University gratefully acknowledge financial support from the Department of Science and Technology, Government of India. K.R.P. and P.R.S. thank Grant-in-Aid for Scientific Research Category S. No. 16106010 for financial support to carry out EXAFS experiments and PF Advisory Committee (PAC) Approval for approval of the project. P.R.S. would like to thank Hokkaido University for a Visiting Professorship.

[1] P. Bera, K. C. Patil, V. Jayaram, G. N. Subbanna, and M. S. Hegde, J. Catal. **196**, 293 (2000).
[2] K. R. Priolkar, P. Bera, P. R. Sarode, M. S. Hegde, S. Emura, R. Kumashiro, and N. P. Lalla, Chem. Mater. **14**, 2120 (2002).
[3] P. Bera, K. R. Priolkar, P. R. Sarode, M. S. Hegde, S. Emura, R. Kumashiro, V. Jayaram, and N. P. Lalla, Chem. Mater. **14**, 3591 (2002).
[4] P. Bera, K. R. Priolkar, A. Gayen, P. R. Sarode, M. S. Hegde, S. Emura, R. Kumashiro, V. Jayaram, and G. N. Subbanna, Chem. Mater. **15**, 2049 (2003).
[5] A. Gayen, K. R. Priolkar, P. R. Sarode, V. Jayaram, M. S. Hedge, G. N. Subbanna, and S. Emura, Chem. Mater. **16**, 2317 (2004).
[6] P. Bera, A. Gayen, M. S. Hegde, N. Lalla, L. Spadaro, F. Frusteri, and F. Arena, J. Phys. Chem. B **107**, 6122 (2003).
[7] *Catalysis by Ceria and Related Materials*, edited by A. Trovarelli (Imperial College Press, London, 2002).
[8] E. Mamontov, T. Egami, R. Brezny, M. Koranne, and S. Tyagi, J. Phys. Chem. B **104**, 11110 (2000).
[9] P. Fornasiero, G. Balducci, R. De Monte, J. Kaspar, V. Sergo, G. Gubitosa, A. Ferrero, and M. Graziani, J. Catal. **164**, 173 (1996).
[10] P. Fornasiero, E. Fonda, R. De Monte, G. Vlaic, J. Kašpar, and M. Graziani, J. Catal. **177**, 187 (1999).
[11] E. Bekyarova, P. Fernasiero, J. Kašpar, and M. Graziani, Catal. Today **45**, 179 (1998).
[12] T. Baidya, A. Gayen, M. S. Hegde, N. Ravishankar, and L. Dupont, J. Phys. Chem. B **110**, 5262 (2006).
[13] G. Dutta, U. V. Waghmare, T. Baidya, M. S. Hedge, K. R. Priolkar, and P. R. Sarode, Chem. Mater. **18**, 3249 (2006).
[14] T. Baidya, A. Marimuthu, M. S. Hegde, N. Ravishankar, and G. Madras, J. Phys. Chem. C **111**, 830 (2007).
[15] R. A. Young, *The Rietveld Method* (Oxford University Press, New York, 1995).
[16] M. Nomura and A. Koyama, Nucl. Instrum. Methods Phys. Res. A **467–468**, 733 (2001).
[17] M. Nomura, Y. Koike, M. Sato, A. Koyama, Y. Inada, and K. Asakura, AIP Conf. Proc. **882**, 896 (2007).
[18] E. A. Stern and K. Kim, Phys. Rev. B **23**, 3781 (1981).
[19] W. P. Pearson, *Handbook of Lattice Spacing and Structure of Metals and Alloys* (Pergamon, New York, 1958).
[20] S. I. Zabinsky, J. J. Rehr, A. Ankudinov, R. C. Albers, and M. J. Eller, Phys. Rev. B **52**, 2996 (1995).
[21] E. A. Stern, M. Newville, B. Ravel, Y. Yacoby, and D. Haskel, Physica B **208–209**, 117 (1995).
[22] Y. Nishihata, J. Mizuki, T. Akao, H. Tanaka, M. Uenishi, M. Kimura, T. Okamoto, and N. Hamada, Nature (London) **418**, 164 (2002).
[23] H. Tanaka, M. Taniguchi, M. Uenishi, N. Kajita, I. Tan, and Y. Nishihata, Angew. Chem., Int. Ed. **45**, 5998 (2006).
[24] J. Li, U. G. Singh, J. W. Bennett, K. Page, J. C. Weaver, Z.-P. Zhang, T. Proffen, A. M. Rappe, S. Scott, and R. Seshadri, Chem. Mater. **19**, 1418 (2007).
[25] D. Briggs and M. P. Seah, *Practical Surface Analysis* (Wiley, New York, 2004).
[26] P. Bera, K. R. Priolkar, A. Gayen, P. R. Sarode, M. S. Hegde, S. Emura, R. Kumashiro, V. Jayaram, and G. N. Subbanna, Chem. Mater. **14**, 3591 (2002).